Generalized Koebe's Method for Conformal Mapping Multiply Connected Domains

Wei Zeng Xiaotian Yin Min Zhang
Stony Brook University
{zengwei|xyin|mzhang}@cs.sunysb.edu

Feng Luo
Rutgers University
fluo@math.rutger.edu

Xianfeng Gu
Stony Brook University
gu@cs.sunysb.edu

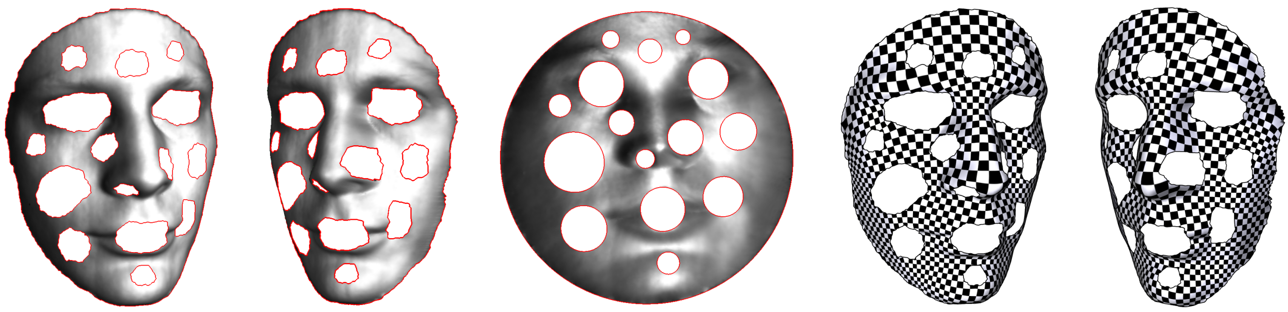

(a) Left-view (b) Right-view (c) Circular conformal map (d) Checkerboard (e) Checkerboard

Figure 1: Conformal mapping for multiply connected domains. A human face surface with 15 holes is mapped to the unit disk with circular holes. (a-b): the input surfaces captured from left-view and right-view. (c): the input surface is conformally mapped to a circular domain, where all the holes are mapped to circles. (d-e): the checkerboard texture is mapped to the input surface by the conformal parametrization from (c). The conformality of mapping is visualized by the checkerboard texture mapping, where the right angles are preserved well.

Abstract

Surface parameterization refers to the process of mapping the surface to canonical planar domains, which plays crucial roles in texture mapping and shape analysis purposes. Most existing techniques focus on simply connected surfaces. It is a challenging problem for multiply connected genus zero surfaces. This work generalizes conventional Koebe's method for multiply connected planar domains. According to Koebe's uniformization theory, all genus zero multiply connected surfaces can be mapped to a planar disk with multiply circular holes. Furthermore, this kind of mappings are angle preserving and differ by Möbius transformations. We introduce a practical algorithm to explicitly construct such a *circular conformal mapping*. Our algorithm pipeline is as follows: suppose the input surface has n boundaries, first we choose 2 boundaries, and fill the other $n - 2$ boundaries to get a topological annulus; then we apply discrete Yamabe flow method to conformally map the topological annulus to a planar annulus; then we remove the filled patches to get a planar multiply connected domain. We repeat this step for the planar domain iteratively. The two chosen boundaries differ from step to step. The iterative construction leads to the desired conformal mapping, such that all the boundaries are mapped to circles. In theory, this method converges quadratically faster than conventional Koebe's method. We give theoretic proof and estimation for the converging rate. In practice, it is much more robust and efficient than conventional non-linear methods based on curvature flow. Experimental results demonstrate the robustness and efficiency of the method.

CR Categories: I.3.5 [Computing Methodologies]: Computer Graphics—Computational Geometry and Object Modeling; G.2.1 [Mathematics of Computing]: Discrete Mathematics—Combinatorics

Keywords: Conformal, Holomorphic, Differential Form, Uniformization, Circular, Multiply Connected Domain

1 Introduction

Surface parameterization refers to the process of mapping a surface embedded in $\mathbb{R}^3$ to a canonical planar domain with minimal distortions. In general, distortions can be classified according to angle distortion and area distortion. Conformal parameterizations are desirable for engineering applications, because there are free of angle distortion. Conformal parameterization plays an important role in shape modeling, synthesis and analysis. It has broad applications in computer-aided design, engineering and manufacturing. It also has been applied for texture mapping in graphics, surface registration in computer vision, brain mapping and colonoscopy in medical imaging fields.

Most existing conformal parameterization methods can only handle simply connected surfaces, namely topological disks without holes inside. In practice, most shapes have complicated topologies. For example, due to the occlusion, most surface directly acquired from real life using 3D scanners are *multiply connected domains*, namely a genus zero surface with multiple holes. According to Koebe's uniformization theory in differential geometry, it can be conformally mapped to the unit disk with circular holes. If we fix the images of an interior point and a boundary point, the mapping is unique. This kind of mapping is called the *conformal uniformization* of multiply connected domains. Figure 1 shows one example, a human face surface with 15 holes in frames (a-b) that is mapped to the unit disk with circular holes in frame (c). The conformality of the mapping can be verified in frames (d-e) by texture mapping a checkerboard image onto the surface induced by the conformal mapping. It is easy to see that all the right angles of the checkers are well-preserved.

Computing the conformal uniformization for disks with multiple holes is very challenging. For the existing linear harmonic map and least-square conformal map, if the target domain is non-convex, the map may not be a homeomorphism. So far, the only practical method in the literature which is able to construct the canonical conformal mapping for genus zero surfaces with holes in $\mathbb{R}^3$ is discrete curvature flow method, including both discrete Ricci flow and discrete Yamabe flow. Unfortunately, there are two major drawbacks of discrete curvature flow methods for computing the uniformization of multiply connected domains:

1. **Robustness**: If the triangulation quality is not good enough, the curvature flow methods will get stuck (see the not-converge cases in Table 1). Especially, the curvature flow methods are vulnerable to meshes scanned in real life due to their low triangulation qualities. Although in theory, the existence of the solution is determined by the connectivity of the mesh, there is no practical algorithm to predict whether the discrete curvature flow will lead to the solution or encounter singularities in the middle.
2. **Efficiency**: Curvature flow methods are highly non-linear, for large meshes, the computations are highly expensive.

1.1 Motivation

Surfaces can be classified by the conformal equivalence relation. Two surfaces are conformally equivalent if there exists a conformal map between them. For multiply connected domains, they are conformally equivalent, if and only if their conformal parametric domains differ by a Möbius transformation. Circular boundary is highly preferred for shape analysis purpose. In this work, the boundaries are mapped to circles by conformal maps, which will give us the well defined shape fingerprints, which are the centers and radii. The positions of the circles are determined by the geometry of the surface automatically. The fingerprints are conformal invariants, called conformal modules [Zeng et al. 2009b], which are invariant up to Möbius transformation. The major motivation of this work is for shape analysis purposes, including shape indexing, shape comparison, shape registration, etc.

In order to process large meshes with low quality of triangulations in engineering applications, more robust and efficient algorithms need to be developed.

1.2 Generalized Koebe's Method

The main contribution of this work is to present a novel iterative method to compute the conformal uniformizations for multiply connected domains, based on Koebe's method.

Iteration and Step For one *step*, we select two holes, and fill all the other holes, then conformally map the annulus to the canonical planar annulus by solving two linear systems. For one *iteration*, if there are n holes, we choose a different pair of them in each step. We go through all the n holes after $n/2$ steps, which form one iteration.

Our method has the following merits:

1. **Robustness**: it is much more robust than curvature flow method. It tolerates the triangulations with poor qualities.
2. **Efficiency**: Each iteration is a linear procedure, and in practice it requires only a couple of linear steps. Therefore, it is much faster than curvature flow method.
3. **Rigor**: The method is rigorous, we give theoretic proof for the analysis for converging rate in the Appendix.

The method is based on conventional Koebe's method.

Conventional Koebe's Method Figure 2 illustrates the conventional Koebe's method for conformal uniformization of multiply connected domains. The input surface S is shown in the first frame of the top row, which has 4 boundaries

$$\partial S = \gamma_0 - \gamma_1 - \gamma_2 - \gamma_3.$$

Then a conformal mapping $\phi_1 : S \to \mathbb{D}$ is computed, where $\mathbb{D}$ is the unit disk, such that ϕ_1 maps γ_0 to the unit circle. The image $\phi_1(S)$ is shown in frame (1). Then another conformal mapping is computed $\phi_2 : \phi_1(S) \to \mathbb{D}$, such that γ_2 is mapped to the circle. The image of ϕ_2 is shown in frame (2). Then a conformal mapping $\phi_3 : \phi_2 \circ \phi_1(S) \to \mathbb{D}$ is computed, which maps γ_3 to the unit circle. At the k-th step, we can get conformal mapping

$$\phi_k : \circ\phi_{k-1} \circ \cdots \circ \phi_1(S) \to \mathbb{D}$$

which maps a boundary loop to the unit circle. Then the compositions of the mappings ϕ_k's converge to the desired conformal mapping with appropriate normalization conditions.

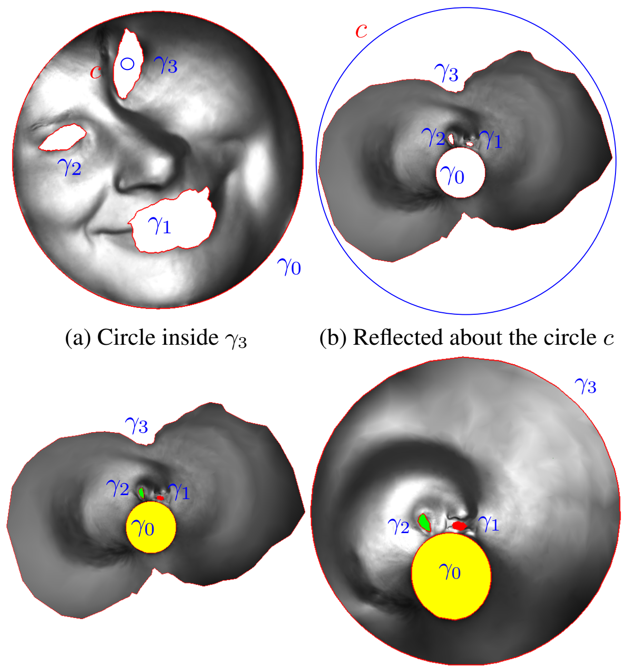

(a) Circle inside γ_3 (b) Reflected about the circle c

(c) Fill inner holes (d) Conformal mapping

Figure 3: Find a conformal mapping to map γ_3 to the unit circle.

Figure 3 explains how to find a conformal mapping $\phi_2 : \phi_1(S) \to \mathbb{D}$, such that $\phi_2(\gamma_3)$ is the unit circle. First, a circle c inside γ_3 is found in $\phi_1(S)$ as shown in frame (a); Second, the reflection of the whole complex plane about the circle c is computed, denoted as τ. Then γ_3 is transformed to the exterior boundary as shown in frame (b); Third, fill all the inner holes bounded by γ_0 (yellow), γ_1 (red) and γ_2 (green); At last, a Riemann mapping ϕ is computed, which maps the domain in frame (c) to the unit disk in frame (d). Then the desired conformal mapping ϕ_2 is given by $\phi \circ \tau$. Note that, in the input domain, $\phi_1(\gamma_0)$ is a circle. After the mapping, $\phi_2(\phi_1(\gamma_0))$ is still close to a circle. In the iterations, all the boundaries are getting rounder and rounder, and eventually become circles.

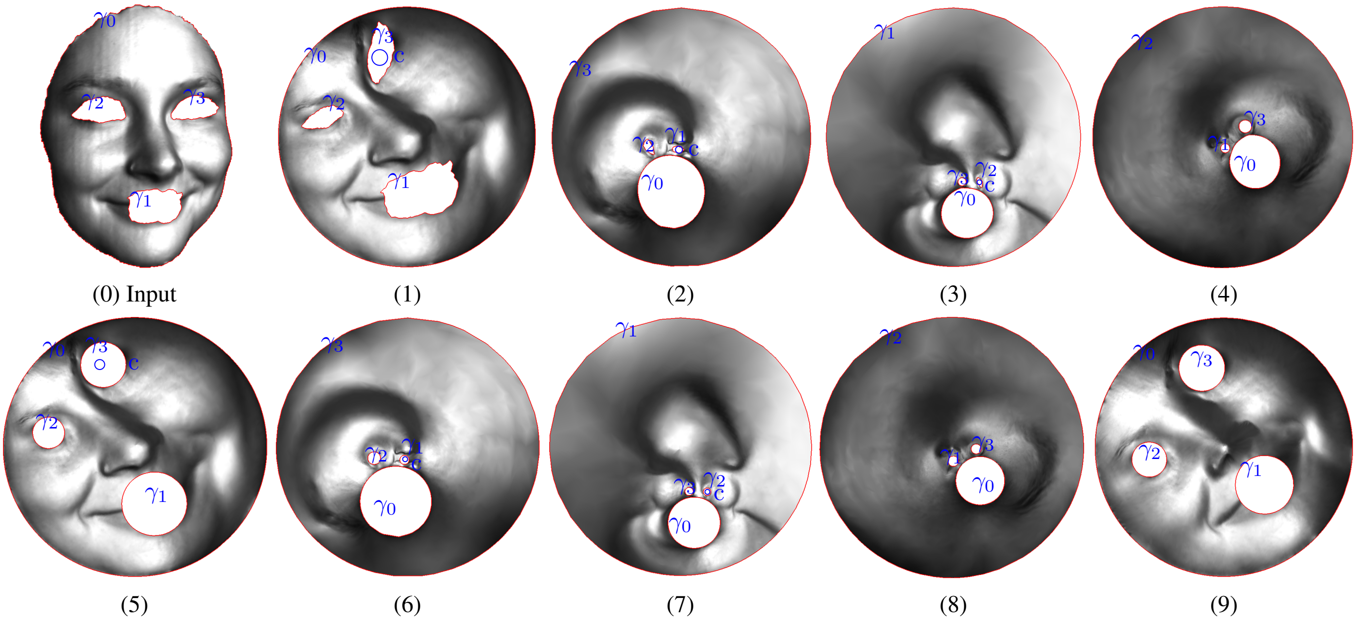

Figure 2: Conventional Koebe's method (**CK**). Steps (0-4): Iteration 1; Steps (5-9): Iteration 2. In each step, one boundary is chosen to be mapped to the exterior circle. In each iteration, the boundary is chosen in the following order: $\gamma_0, \gamma_3, \gamma_1, \gamma_2$.

Let p be a interior point of S. We can easily construct a Möbius transformation from the complex plane to itself $\tau(z) = \frac{1}{z-p}$. Then τ transforms all the boundaries to be interior boundaries. Denote $\tau(S)$ as $\tilde{S}$. Let $f_k = \phi_k \circ \phi_{k-1} \cdots \phi_1 \circ \tau^{-1}$, then by using Möbius transformations we can normalize f_k, such that

$$f_k(\infty) = \infty, f_k(z) = z + O(z^{-1}), \quad (1)$$

near the ∞ point. Let $f : \tilde{S} \to \mathbb{C}$ by the conformal uniformization map, which satisfies the normalization condition in 1. Then the following theorem gives the convergence estimation explicitly,

Theorem 1.1 (Henrici). *Suppose the planar surface has n boundaries, then there exist constants $C_1 > 0$, $0 < C_2 < 1$, for step k, for all $z \in \mathbb{C}$,*

$$|f_k \circ f^{-1}(z) - z| < C_1 C_2^{[\frac{k}{n}]}$$

Here $[\frac{k}{n}]$ denotes the greatest integer not exceeding $\frac{k}{n}$. The detailed proof can be found in [Henrici 1993], theorem 17.7a.

Generalized Koebe's Method The *generalized Koebe's method* differs from conventional ones by the following face: at each step, conventional Koebe's algorithm deforms **one** boundary to a circle; whereas, generalized Koebe's algorithm deforms **two** boundaries to circles. The computational costs for each step of conventional method and generalized method are almost the same and generalized method converges much faster and requires much fewer iterations. Therefore, the new method is much more efficient. Figure 4 demonstrates the computational process of the same surface as in Figure 2. From the roundness of the boundaries, it is easy to tell that the generalized Koebe method converges much faster than conventional method.

In one word, the generalized Koebe's method makes great improvements in the following aspects

1. **Generality** Conventional Koebe's algorithm handles the planar regions, this method is generalized to handle surfaces in $\mathbb{R}^3$.
2. **Efficiency** This method converges quadratically faster than conventional Koebe's method.

Theorem 1.2 (Generalized Koebe). *Suppose genus zero surface has n boundaries, then there exists constants $\gamma > 0$, $0 < \mu < 1$, for step k, for all $z \in \mathbb{C}$,*

$$|f_k \circ f^{-1}(z) - z| < C_1 C_2^{2[\frac{k}{n}]}$$

We give the proof in the Appendix.

2 Previous Works

Recently, with the development of digital scanning technology, computing conformal mappings between surfaces becomes more and more important. In computer graphics and discrete mathematics, much sound research has focused on discrete conformal mappings.

The computational method of current work is mainly based on harmonic maps and holomorphic differential forms. Here, we briefly overview most related work, and refer readers to [Floater and Hormann 2005; Kraevoy and Sheffer 2004] for thorough surveys.

Discrete harmonic maps were constructed in [Pinkall and Polthier 1993], where the cotan formula was introduced. First order finite element approximations of the Cauchy-Riemann equations were introduced by Levy et al. [Lévy et al. 2002]. Discrete intrinsic parameterization by minimizing Dirichlet energy was introduced by [Desbrun et al. 2002]. Mean value coordinates were introduced in [Floater 2003] to compute generalized harmonic maps; Discrete spherical conformal mappings are used in [Gotsman et al. 2003] and [Gu et al. 2004].

Discrete holomorphic forms are introduced in [Gu and Yau 2003] to compute global conformal surface parameterizations for high genus surfaces. Another approach of discrete holomorphy was introduced in [Mercat 2004] using discrete exterior calculus [Hirani 2003]. The problem of computing optimal holomorphic 1-forms to reduce area distortion was considered in [Jin et al. 2004]. [Gortler et al. 2005] generalized 1-forms to the discrete case, using them to parameterize genus one meshes. [Tong et al. 2006b] generalized the 1-form

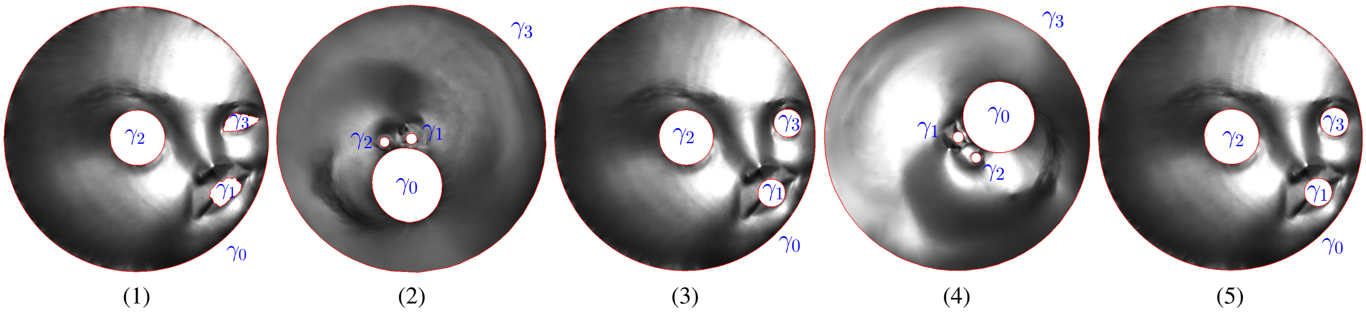

Figure 4: Generalized Koebe's method (**GK**) with faster convergence. In each step, two boundaries are chosen to be mapped to the exterior circle and the interior circle respectively. Step (1): (γ_0, γ_2), Step (2): (γ_3, γ_0), Step (3): (γ_0, γ_2), Step (4): (γ_3, γ_1), and Step (5): (γ_0, γ_2).

method to incorporate cone singularities.[Yin et al. 2008]constructs special holomorphic one forms that map a genus zero surface with multiple holes to an annulus with concentric circular slits. Discrete one-forms have been applied for meshing point clouds in [Tewari et al. 2006], surface tiling [Desbrun 2006], surface quadrangulation [Tong et al. 2006a]. Holomorphic 1-form method has been applied for virtual colonoscopy [Hong et al. 2006]. The colon surface is reconstructed from MRI images, and conformally mapped to the planar rectangle. This improves the efficiency and accuracy for detecting polyps. Conformal mapping is used for brain cortex surface morphology study in [Gu et al. 2004]. By mapping brain surfaces to spheres, cortex surface registration and comparison become straightforward. Holomorphic 1-form method has also been applied in computer vision [Wang et al. 2007; Zeng et al. 2008b] for 3D shape matching, recognition and stitching. In geometric modeling field, constructing splines on general surfaces is one of the most fundamental problems. It is proven in [Gu et al. 2006] that if a surface has an affine structure, then spline can be construct on to it directly. Holomorphic 1-forms can be applied for computing the affine structures of general surfaces.

The Ricci flow was firstly proposed by Hamilton [Hamilton 1982] as a tool to conformally deform the metric according to the curvature. In [Chow and F.Luo 2003] Chow and Luo developed the theories of the combinatorial surface Ricci flow, which was later implemented and applied for surface parameterization [Jin et al. 2006; Jin et al. 2008a], shape classification [Jin et al. 2008b], shape mapping [Li et al. 2008] and surface matching [Zeng et al. 2008a]. Discrete Yamabe flow was introduced by Luo in [Luo 2004]. In a recent work of Springborn et al. [Boris Springborn and Pinkall 2008], the Yamabe energy is explicitly given busing the Milnor-Lobachevsky function. Hyperbolic Yamabe flow has been applied for computing closed geodesics as the canonical representative of a homotopy class in [Zeng et al. 2009a].

So far, only curvature flow method can compute the conformal uniformization of multiply connected domains. Due to the non-linear nature of the curvature flow method, the computation is expensive. This work uses holomorphic 1-form for the computation, which is much more efficient.

3 Theoretic Background

This section briefly introduces the theoretic background for this work. We refer readers to [Guggenheimer 1977; Weitraub 2007] for more details.

3.1 Harmonic Functions

Suppose S is a surface with a Riemannian metric $\mathbf{g}$, f is a function defined on S, $f : S \to \mathbb{R}$. The *harmonic energy* of f is defined as

$$E(f) = \int_S |\nabla f|^2 dv,$$

where ∇f is the gradient of f. A *harmonic function* is a critical point of the harmonic energy, which satisfies the Laplace equation

$$\Delta f = 0,$$

where Δ is the Laplace-Beltrami operator determined by the Riemannian metric.

3.2 Riemann Surface

Let $f : \mathbb{C} \to \mathbb{C}$ be a complex-valued function, $f(x + iy) = u(x, y) + iv(x, y)$. If it satisfies the following Cauchy-Riemann equations:

$$\frac{\partial u}{\partial x} = \frac{\partial v}{\partial y}, \frac{\partial u}{\partial y} = -\frac{\partial v}{\partial x},$$

then it is *holomorphic*. A holomorphic function preserves angles.

Suppose S is a topological surface. As shown in Figure 5, U_α is an open set on the surface. $\phi_\alpha : U_\alpha \to \mathbb{C}$ is homeomorphism, which maps U_α to the complex plane. Then (U_α, ϕ_α) is a *local coordinate chart*. Suppose two local coordinate charts have an overlapping $U_\alpha \bigcap U_\beta$, then the *coordinate transition function* is given by

$$\phi_{\alpha\beta} = \phi_\beta \circ \phi_\alpha^{-1} : \phi_\alpha(U_\alpha \cap U_\beta) \to \phi_\beta(U_\beta \cap U_\alpha).$$

Suppose $\{U_\alpha\}$ form an open covering of the surface, $S \subset \bigcup_\alpha U_\alpha$, then the collection of charts $\{(U_\alpha, \phi_\alpha)\}$ form an *atlas*. If all the coordinates transition functions are holomorphic, then the atlas is called a *conformal structure*, the surface is called a *Riemann surface*.

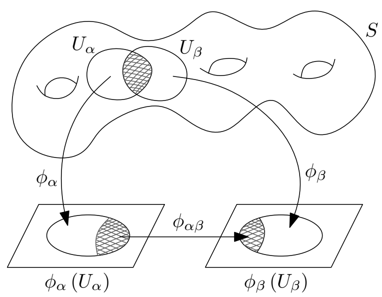

Figure 5: Riemann surface: If all the chart transition functions $\phi_{\alpha\beta}$'s are holomorphic, the surface is a Riemann surface.

Intuitively, given two curves on a Riemann surface, one can measure their intersection angle in a chart. The measurement is independent of the choice of the chart. Therefore, angles are well defined on a Riemann surface.

Let S be a surface embedded in $\mathbb{R}^3$, then it has an induced Euclidean metric $\mathbf{g}$. Let (U_α, ϕ_α) be a local coordinates chart with local parameters (u_α, v_α), if

$$\mathbf{g} = e^{2\lambda(u_\alpha, v_\alpha)}(du_\alpha^2 + dv_\alpha^2),$$

then the local coordinates are called *isothermal coordinates*. Then one can use isothermal coordinates to build an atlas, which gives a conformal structure of the surface. Therefore all metric surfaces are Riemann surfaces.

3.3 Holomorphic 1-form

Let S be a Riemann surface with a conformal atlas, the local parameter for the chart (U_α, ϕ_α) be z_α. A *holomorphic 1-form* has the local representation

$$\omega = f_\alpha(z_\alpha)dz_\alpha,$$

where f_α is a holomorphic function. On another chart (U_β, ϕ_β), ω has the local representation $f_\beta(z_\beta)dz_\beta$, such that

$$f_\alpha \frac{dz_\alpha}{dz_\beta} = f_\beta.$$

All holomorphic 1-forms on a Riemann surface form a group $\Omega^{1,0}(S)$, which is isomorphic to the first cohomology group of the surface.

Each holomorphic 1-form ω can be represented as a pair of *harmonic 1-forms*,

$$\omega = \tau + \sqrt{-1}^* \tau,$$

where * is the *Hodge star* operator (see [Gu and Yau 2003] for the computating details).

The follows are the local representations of τ and its conjugate $^*\tau$

$$\tau = g_\alpha dx_\alpha + h_\alpha dy_\alpha, {}^*\tau = g_\alpha dy_\alpha - h_\alpha dx_\alpha.$$

The *exterior derivative* of τ is given by

$$d\tau = (\frac{\partial h_\alpha}{\partial x_\alpha} - \frac{\partial g_\alpha}{\partial y_\alpha})dx_\alpha \wedge dy_\alpha.$$

If $d\tau$ is zero, then τ is a *closed 1-form*.

The *exterior co-derivative* operator is defined as

$$\delta = {}^*d^*.$$

Furthermore, if $\delta\tau$ is also closed, then τ is a *harmonic 1-form*. Locally, a harmonic 1-form is the derivative of a harmonic function. Hodge theory postulates the existence and the uniqueness of harmonic forms in each cohomologous class.

Theorem 3.1 (Hodge). *Each cohomologous class has a unique harmonic differential form.*

3.4 Conformal Mappings

Let S_1 and S_2 be two Riemann surfaces with conformal structures $\{(U_\alpha, \phi_\alpha)\}$ and $\{(V_\beta, \eta_\beta)\}$. A map $f : S_1 \to S_2$ is *conformal*, if its local presentation

$$\eta_\beta \circ f \circ \phi_\alpha^{-1} : \phi_\alpha(U_\alpha) \to \eta_\beta(V_\beta)$$

is holomorphic.

If S_1 and S_2 are metric surfaces, with Riemannian metrics $\mathbf{g}_1$ and $\mathbf{g}_2$ respectively, then f is conformal, if and only if the pull back metric induced by f satisfies

$$f^*\mathbf{g}_2 = e^{2\lambda}\mathbf{g}_1.$$

All the conformal mappings from the unit disk to itself can be represented as a *Möbius transformation*,

$$z \to e^{i\theta}\frac{z - z_0}{1 - \bar{z}_0 z}, z_0, z \in \mathbb{D},$$

where $\mathbb{D}$ is the unit disk on the complex plane $|z| < 1$.

Our current work focuses on the conformal uniformization theorem for multiply connected domains,

Theorem 3.2 (Uniformization). *Suppose S is a genus zero surface with multiple boundaries, and a Riemannian metric $\mathbf{g}$. There exists a conformal map $f : S \to D$, where D is the unit disk with circular holes. Two such kind of mappings differ by a Möbius transformation.*

4 Computational Algorithm

4.1 Discrete Approximation

Here we briefly introduce the discrete approximation for surface, forms, and harmonic 1-form. For more details of computational algorithm, we refer readers to [Gu and Yau 2003].

Surface In practice, surfaces are approximated by simplicial complexes (triangle meshes) embedded in $\mathbb{R}^3$. Suppose M is a triangle mesh with vertex set V, oriented edge set E and oriented face set F. The i-th vertex is denoted as v_i, the oriented edge from v_i to v_j is $[v_i, v_j]$, the oriented face with vertices v_i, v_j, v_k sorted counter-clock-wisely is $[v_i, v_j, v_k]$. The boundary operator ∂ takes the boundary of simplicies,

$$\partial[v_0, v_1] = v_1 - v_0, \partial[v_0, v_1, v_2] = [v_0, v_1] + [v_1, v_2] + [v_2, v_0].$$

Discrete forms A function defined on the surface is defined on vertices $f : V \to \mathbb{R}$, a 1-form is defined as a function on oriented edges $\omega : E \to \mathbb{R}$, a 2-form is defined as a function on oriented faces $\tau : F \to \mathbb{R}$. The exterior differential operator d is defined as the dual to boundary operator. For a zero form f, df is a 1-form,

$$df([v_0, v_1]) = f(\partial[v_0, v_1]) = f(v_1) - f(v_0).$$

For a 1-form ω, $d\omega$ is a 2-form, $d\omega([v_0, v_1, v_2])$ equals to

$$\omega(\partial[v_0, v_1, v_2]) = \omega([v_0, v_1]) + \omega([v_1, v_2]) + \omega([v_2, v_0]).$$

Discrete Harmonic 1-form Let $[v_i, v_j]$ be an interior edge on the mesh, connecting two faces $[v_i, v_j, v_k]$ and $[v_j, v_i, v_l]$, the corner angle in $[v_i, v_j, v_k]$ against $[v_i, v_j]$ is θ_k^{ij}, the corner angle in $[v_j, v_i, v_l]$ against $[v_i, v_j]$ is θ_l^{ij}, the *edge weight* is defined as

$$w_{ij} = \cot\theta_k^{ij} + \cot\theta_l^{ij},$$

The *discrete harmonic energy* is defined as

$$E(f) = \sum_{[v_i, v_j] \in E} w_{ij}(f(v_i) - f(v_j))^2.$$

The *discrete harmonic function* is the critical point of the harmonic energy, which satisfies the following *discrete Laplace equation*

$$\Delta f(v_i) = \sum_{[v_i, v_j] \in E} w_{ij}(f(v_j) - f(v_i)) = 0, \forall v_i \in V. \quad (2)$$

Let ω be a *discrete harmonic 1-form*, then it satisfies the following condition

$$\delta\omega(v_i) = \sum_{[v_i, v_j] \in E} w_{ij}\omega([v_i, v_j]) = 0, \forall v_i \in V. \quad (3)$$

4.2 Doubly Connected Domain

Suppose S is a topological annulus, with boundaries $\partial S = \gamma_0 - \gamma_1$ as shown in Figure 6.

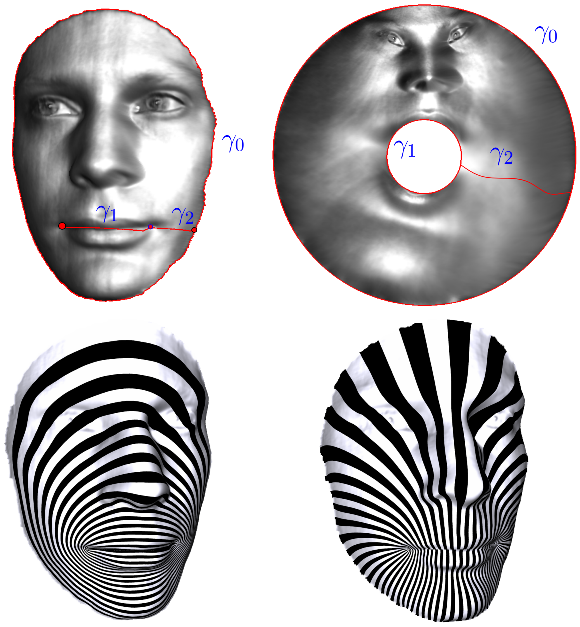

Figure 6: Harmonic 1-forms. Top row, the cut on the surface and its conformal annulus mapping. Bottom row, the level sets of the harmonic 1-form df and its conjugate harmonic 1-form $\lambda(dg_0 + dg_1)$.

First, we compute a path γ_2 connecting γ_0 and γ_1. Then we compute a harmonic function $f : S \to \mathbb{R}$, such that

$$\left\{ \begin{array}{lcl} f_{\gamma_0} & = & 0 \\ f_{\gamma_1} & = & 1 \\ \Delta f & = & 0 \end{array} \right.$$

The level set of f is shown in Figure 6. Then df is a harmonic 1-form.

We slice the surface along γ_2 to get a new surface $\tilde{S}$ with a single boundary. γ_2 becomes two boundary segments γ_2^+ and γ_2^- on $\tilde{S}$. Then we compute a function $g_0 : \tilde{S} \to \mathbb{R}$, such that

$$\left\{ \begin{array}{lcl} g_0|_{\gamma_2^+} & = & 1 \\ g_0|_{\gamma_2^-} & = & 0 \end{array} \right.$$

g_0 takes arbitrary value on other vertices. Therefore dg_0 is a closed 1-form defined on S. Then we find another function $g_1 : S \to \mathbb{R}$, such that $dg_0 + dg_1$ is a harmonic 1-form $\delta(dg_0 + dg_1) = 0$.

Then we need to find a scalar λ , such that ${}^*df = \lambda(dg_0 + dg_1)$, using the similar method as for topological quadrilaterals. The holomorphic 1-form is given by

$$\omega = df + \sqrt{-1}\lambda(dg_0 + dg_1).$$

Let $Img(\int_{\gamma_0} \omega) = k$, The conformal mapping from S to a canonical annulus is given by

$$\phi(p) = \exp^{\frac{2\pi}{k}\int_q^p \omega},$$

where q is the base point, the path from q to p is arbitrarily chosen.

4.3 Simply Connected Domain

For a surface S which is a simply connected domain as shown in Figure 7, the conformal mapping can be computed straightforwardly.

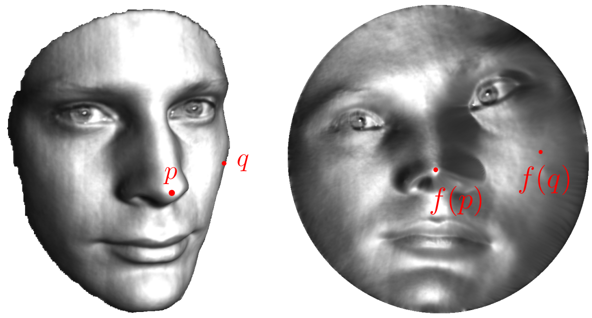

Figure 7: Riemann mapping using holomorphic 1-form.

We choose an interior point $p \in S$, and a boundary point $q \in \partial S$. We choose a sequence of small disks D_n, such that
(a). $D_0 \supset D_1 \supset D_2 \supset \cdots$,
(b). $\lim_{n\to\infty} diagmeter(D_n) = 0$,
(c). $\bigcap_{n=0}^{\infty} D_n = p$.
Then we compute a conformal mapping $f_n : S - D_n \to \mathbb{D}$, where $\mathbb{D}$ is the unit disk, the boundary of D_n is mapped to a concentric circle, furthermore $f_n(q) = 1$. Then $\{f_n\}$ form a normal family, we can prove the following

Theorem 4.1. *The mappings $\{f_n\}$ converge to the Riemann mapping $f : S \to \mathbb{D}$*

$$\lim_{n\to\infty} f_n = f,$$

such that f maps p to the origin, q to 1.

4.4 Multiply Connected Domains

Suppose the input surface is a genus zero surface with multiple holes. We apply the generalized Koebe's method to compute the canonical conformal mappings, or uniformize them. Computing the conformal mapping of multiply connected domains is reduced to compute the conformal mapping of a topological annulus, which is equivalent to compute a pair of conjugated harmonic 1-forms.

Hole Filling There are many ways to fill holes on surfaces, such as the method in [Xu 2008]. In our case, the shapes of the filled surface patches won't affect the result quality. Then we adopted the following simple method: For each boundary loop, we add one central vertex, which is the mass center of all the vertices on the boundary; then each edge on the loop and the center vertex forms a triangle. After the first step the surface is mapped onto the plane; then we use planar mesh generation method based on Delaunay triangulation to fill planar patches.

As shown in Figure 8, the frame (a) is the input surface, which is a genus zero surface with three holes, the boundary of the surface are $\partial S = \gamma_0 - \gamma_1 - \gamma_2 - \gamma_3$. The frame (c) shows that the surface holes are filled with topological disks D_1, D_2 and D_3. The conformal mappings of (a) and (c) are shown in frames (b) and (d), where the surface is mapped to the unit disk with circular holes.

Figure 9 shows the computational process. The following routine handles one disk D_k, as shown in one row of the figure.

1. Remove a disk D_k from $\tilde{S}$, shown in the frames in the first column.

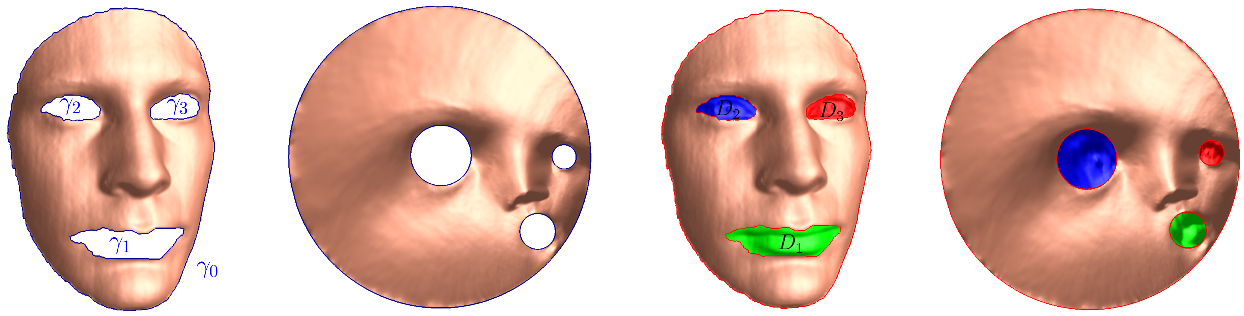

(a) Input (b) Conformal mapping of (a) (c) Holes filling (d) Conformal mapping of (c)

Figure 8: Conformal mapping for Koebe's method.

2. Conformally map the annulus to the canonical annulus, such that the boundary γ_k is mapped to a circle c_k,

$$\phi_k : \tilde{S} - D_k \to \mathbb{D},$$

such that $\phi_k(\gamma_k) = c_k$, as shown in the frames in the second column.

3. Compute a harmonic map of D_k, with the boundary condition that the boundary of D_k is mapped to c_k,

$$f_k : D_k \to \mathbb{D}, \Delta f_k = 0, f_k|_{\gamma_k} = c_k.$$

shown in the frames in the third column.

4. Update the whole mesh $\tilde{S}$,

$$\tilde{S} \leftarrow \phi_k(\tilde{S} - D_k) \cup f_k(D_k).$$

The whole algorithm is as follows:

1. Process D_1, D_2, D_3 respectively using the above algorithm, after this iteration, the boundary of each disk is mapped to a circular curve, compute the center and the radii as (c_k, r_k), as shown in the first three rows in Figure 9.

2. Repeat step 1 until the process converges. The termination condition is given by:

$$\sum_{k=1}^{3} |c_k^0 - c_k^1|^2 + |r_k^0 - r_k^1|^2 < \epsilon,$$

where (c_k^0, r_k^0) and (c_k^1, r_k^1) are the center and radius of D_k of two consecutive iterations.

Figure 9 shows the first two iterations, the circles of all the boundaries are very similar already.

In the previous method, the boundary γ_0 is not filled by a disk and always mapped to the unit circle in the process. In fact, γ_0 can also be filled and treated as the same other boundaries. This will further improve the efficiency.

1. Given a multiply connected domain S with $n+1$ boundaries, fill all boundaries γ_k's with topological disks D_k's,

$$\partial D_k = \gamma_k, k = 0, 1, \cdots, n.$$

The resulting surface is a topological sphere

$$\tilde{S} = S \cup D_0 \cup D_1 \cup \cdots \cup D_n.$$

2. Remove two disks D_i and D_j from $\tilde{S}$, denote the annulus as

$$\tilde{S}_{ij} = \tilde{S}/\{U_i \cup U_j\}.$$

3. Map the annulus $\tilde{S}_{ij}$ to a canonical planar annulus, such that γ_i is mapped to the unit circle, γ_j is mapped to a concentric inner circle, denote the map as $\phi : \tilde{S}_{ij} \to \mathbb{D}$. Replace $\tilde{S}_{ij}$ by its image $\phi(\tilde{S}_{ij})$,

$$\tilde{S}_{ij} \leftarrow \phi(\tilde{S}_{ij}).$$

4. Choose another two disks D_k and D_l, further remove them from $\tilde{S}_{ij}$, denote the three hole annulus as

$$\tilde{S}_{ijkl} = \tilde{S}_{ij}/\{D_k \cup D_l\}.$$

5. Compute a small circle (c_k, r_k) inside γ_k. Translate and scale the whole plane to transform the circle to be the unit circle. Reflect $\tilde{S}_{ijkl}$ with respect to the unit circle, $\tau : \mathbb{C} \to \mathbb{C}$, for all $z \in \mathbb{C}$,

$$\tau(z) - c_k = \frac{1}{|z - c_k|^2}(z - c_k).$$

Update $\tilde{S}_{ijkl}$ by its image

$$\tilde{S}_{ijkl} \leftarrow \phi(\tilde{S}_{ijkl}).$$

6. Fill the holes γ_i in $\tilde{S}_{ijkl}$ with D_i by a harmonic map $\phi_i : D_i \to \mathbb{D}$ using γ_i as the boundary condition, namely

$$\Delta\phi_i \equiv 0, \phi(\partial D_i) = \gamma_i.$$

Similarly, fill the hole γ_j with D_j by a harmonic map $\phi_j : D_j \to \mathbb{D}$ using γ_j as boundary condition. Update

$$\tilde{S}_{kl} \leftarrow \tilde{S}_{ijkl} \cup \phi_i(D_i) \cup \phi_j(D_j).$$

7. Repeat step 4 through 6, until the process converges.

This algorithm converges much faster than the previous one. Figure 10 shows the computational process for conformal mapping a human face surface with 5 holes. The first frame (at the top left) is the input surface, the last frame (at the bottom right) shows the conformal parameterization result, transformed by a Möbius transformation.

5 Experimental Results

We implemented the generalized Koebe's method (GK) using generic C++ language on Windows platform. The sparse linear systems are solved using Matlab C++ library. The computational time is tested on the laptop with 2.00GHz CPU, 3.00G RAM.

The geometric data sets are scanned from real human face with high speed and high resolution, phase shifting scanner, as described in

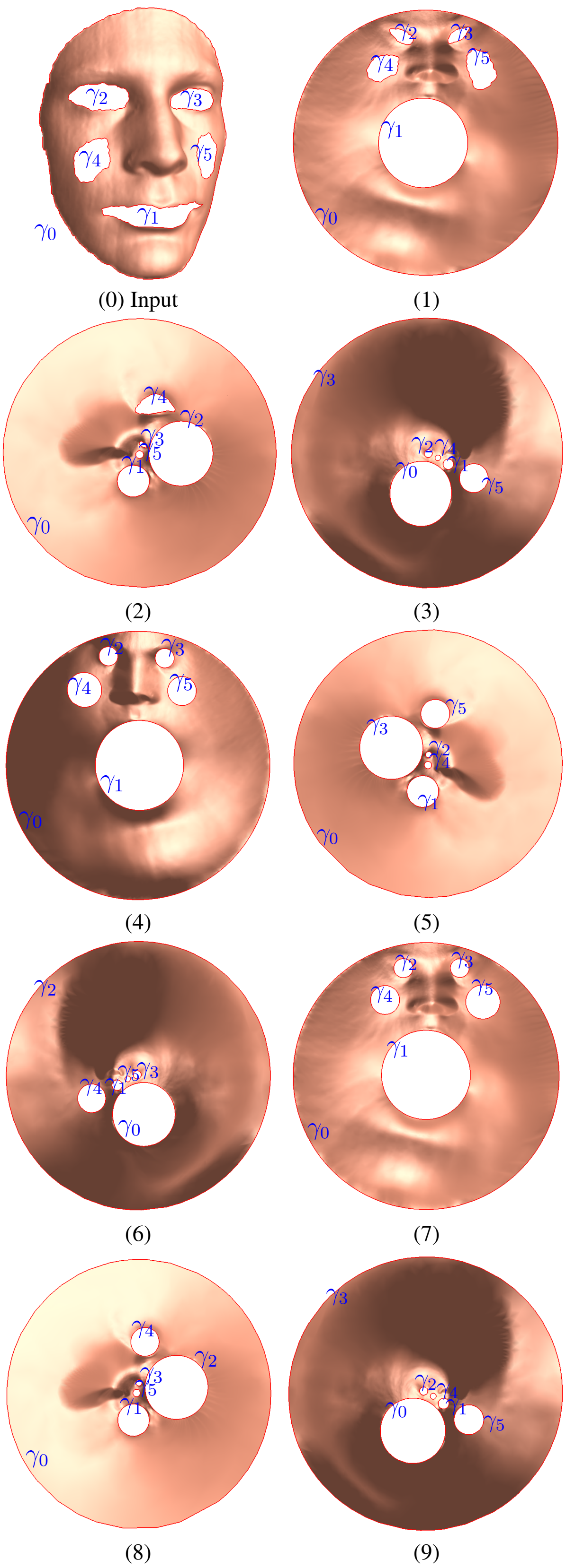

Figure 10: Generalized Koebe's method for computing conformal maps for multiply connected domains with 5 holes. (0): Input surface; (1-9) show the computing process for conformal parameterization transformed by a Möbius transformation.

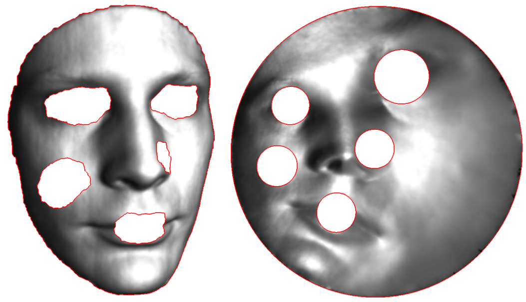

Figure 11: Conformal Mapping for a face surface with 5 holes.

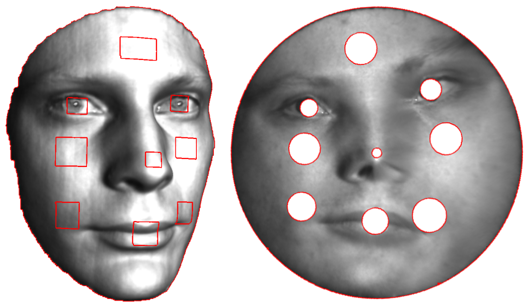

Figure 12: Conformal Mapping for a face surface with 9 holes.

[Wang et al. 2005]. We thoroughly tested our algorithm on several data sets, including two surfaces with 3 holes in Figures 2 and 9, two face with 5 holes in Figures 10 and 11, 9 holes in Figures 12 and 15 holes in Figure 1. The statistics of the experiments are shown in Tables 1 and 2.

Table 1: Comparison for Generalized Koebe's (GK) method and Ricci Flow (RF) method

Model	Fig.2	Fig.8	Fig.10	Fig.11	Fig.12	Fig.1
# H	3	3	5	5	9	15
# V	13515	36737	17732	40335	73839	20226
# F	26304	72391	34653	79999	145566	40034
RF						
T	36	115	45	120	NC	NC
R	0.048356	0.042560	0.044641	0.043786	NC	NC
GK						
# S	42	42	12	6	10	16
T	17	50	14	10	46	16
R	0.040613	0.039315	0.041758	0.037872	0.038551	0.047927

H - hole; V - vertex; F - face; NC - not converge; S - step, T - Time (min); R - Roundness.

Comparison to Curvature Flow Method We compared the generalized Koebe's method with discrete Ricci flow method. In practice, the curvature flow method requires high quality triangulation, and can hardly handle raw meshes generated by 3D scanners. In theory, discrete Yamabe flow is even more vulnerable than discrete Ricci flow (RF). GK is much robust to meshes with degenerated faces and geometric noises. The comparison results are reported in Table 1 in terms of computational time and the roundness for RF and our GK respectively. For surfaces with few holes, such as 3 holes in Figure 8 and 5 holes in Figure 10, the computational speed is improved greatly. For surface with many holes, such as 9 holes in Figure 12 and 15 holes in Figure 1, RF doesn't converge at all. Our experimental results demonstrate the fact that GK is much **faster** and much **more robust** than RF.

Comparison to Conventional Koebe's Method We give the theoretic proof in the Appendix to show that the convergence rate of the generalized Koebe's method is quadratic of that of the conventional Koebe's method (CK). We measure the roundness of the boundary using the following formula. Suppose γ_k consists of a sequence of consecutive vertices $v_1, v_2, \cdots, v_n$, let c be the center of the circle estimated from the vertices, d_i be the distance from the center to v_i, R be the mean of the d_i's. We add a weight w_i to each vertex, which is the ratio between the two adjacent edge lengths and the total edge lengths on the boundary loop. Then the center c is computed as the weighted mass center:

$$c = \frac{1}{n}\sum_{i=1}^{n} w_i v_i, d_i = |v_i - c|, R = \frac{1}{n}\sum_{i=1}^{n} d_i.$$

The measurement for the roundness is defined as

$$e(\gamma_k) = \frac{1}{R}\sqrt{\frac{1}{n}\sum_{i=1}^{n}|d_i - R|^2}.$$

In our experiments, we set the roundness error to be less than a given threshold, and measure the running time using CK and GK, as shown in Table 2. For multi-holed surfaces, we use the average of roundness as the roundness error. In theory, for the same quality of the mapping, the time spent by GK is the **square root** of that of CK. The experiments show that generalized Koebe's mehod is **at least two times faster** than the conventional one.

Table 2: Comparison for Generalized Koebe's (GK) method with Conventional Koebe's (CK) method

Surface	Method	Steps	Time (min)	Roundness
Fig.2	**CK**	9	10.50	0.155102
	GK	5	4.20	0.144580
Fig.8	**CK**	9	34.10	0.144207
	GK	5	8.10	0.143825

Application for Shape Analysis The generalized Koebe's method presents an efficient way to compute the conformal mapping for 3D multiply-connected domains. Based on this, we compute the conformal modules as the fingerprints, which have much potential for the shape analysis purposes. Figure 13 shows the shape indexing and comparison for two faces of different persons with similar expression.

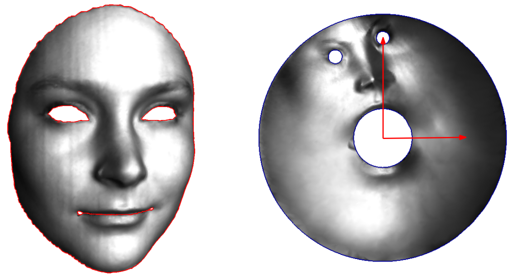

Mod = (0.238, 0.809, 0.053, 0.657, -0.385, 0.055)

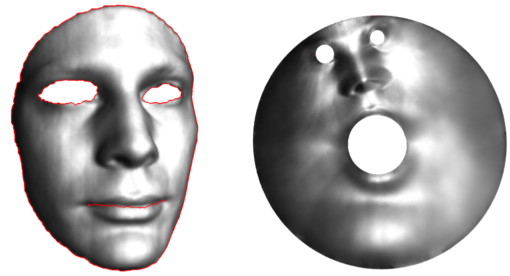

Mod = (0.234, 0.833, 0.057, 0.708, -0.411, 0.073)

Figure 13: Shape analysis by conformal modules for face surfaces with 3 holes. Circle γ_1 denotes the mouth boundary, circles γ_2, γ_3 denote the left and right eyes. After normalization, γ_1 is centered at the origin and the center of γ_2 is on positive y-axis. The conformal module is given as $(r_1, y_2, r_2, x_3, y_3, r_3)$. The distance between two surfaces is the Euclidean distance between their conformal modules.The $L2$ (Euclidean) distance is 0.064952.

6 Conclusion

This work introduces a novel method for constructing conformal mappings, which maps multiply connected domains to the unit disk with circular holes. The method is based on holomorphic 1-form and generalizes conventional Koebe's method. Comparing to the curvature flow method, this method is much more efficient and robust. Comparing to the conventional Koebe's method, this one improves the efficiency, and can handle general surfaces instead of planar domains. Our experimental results demonstrate the efficiency and efficacy of the method.

In the future, we will explore further how to use similar method to compute the conformal mappings for high genus surfaces with boundaries.

Acknowledgments

This work is partially supported by ONR N000140910228, NSF CCF-0841514, NSF CCF-0830550, NSF DMS-0626223. We thank Chris Bishop for the inspiring discussion.

References

BORIS SPRINGBORN, P. S., AND PINKALL, U. 2008. Conformal equivalence of triangle meshes. *ACM Transactions on Graphics 27*, 3, 1–11.

CHOW, B., AND F.LUO. 2003. Combinatorial ricci flows on surfaces. *Journal of Differential Geometry 63*, 1, 97–129.

DESBRUN, M., MEYER, M., AND ALLIEZ, P. 2002. Intrinsic parameterizations of surface meshes. *Computer Graphics Forum (Proc. Eurographics 2002) 21*, 3, 209–218.

DESBRUN, M. 2006. Discrete differential forms and applications to surface tiling. In *SoCG '06: Proceedings of the twenty-second annual symposium on Computational geometry*, ACM, 40–40.

FLOATER, M. S., AND HORMANN, K. 2005. Surface parameterization: a tutorial and survey. In *Advances in Multiresolution for Geometric Modelling*. Springer, 157–186.

FLOATER, M. S. 2003. Mean value coordinates. *Computer Aided Geometric Design 20*, 1, 19–27.

GORTLER, S. J., GOTSMAN, C., AND THURSTON, D. 2005. Discrete oneforms on meshes and applications to 3D mesh parameterization. *Computer Aided Geometric Design 23*, 2, 83–112.

GOTSMAN, C., GU, X., AND SHEFFER, A. 2003. Fundamentals of spherical parameterization for 3d meshes. *ACM Transactions on Graphics 22*, 3, 358–363.

GU, X., AND YAU, S.-T. 2003. Global conformal parameterization. In *Symposium on Geometry Processing*, 127–137.

GU, X., WANG, Y., CHAN, T. F., THOMPSON, P. M., AND YAU, S.-T. 2004. Genus zero surface conformal mapping and its application to brain surface mapping. *IEEE Trans. Med. Imaging 23*, 8, 949–958.

GU, X., HE, Y., AND QIN, H. 2006. Manifold splines. *Graphical Models 68*, 3, 237–254.

GUGGENHEIMER, H. W. 1977. *Differential Geometry*. Dover Publications.

HAMILTON, R. S. 1982. Three manifolds with positive ricci curvature. *Journal of Differential Geometry 17*, 255–306.

HENRICI, P. 1993. *Applide and Computational Complex Analysis, Discrete Fourier Analysis, Cauchy Integrals, Construction of Conformal Maps, Univalent Functions*, vol. 3. Wiley-Interscience.

HIRANI, A. N. 2003. *Discrete exterior calculus*. PhD thesis, California Institute of Technology.

HONG, W., GU, X., QIU, F., JIN, M., AND KAUFMAN, A. E. 2006. Conformal virtual colon flattening. In *Symposium on Solid and Physical Modeling*, 85–93.

JIN, M., WANG, Y., YAU, S.-T., AND GU, X. 2004. Optimal global conformal surface parameterization. In *IEEE Visualization 2004*, 267–274.

JIN, M., LUO, F., AND GU, X. 2006. Computing surface hyperbolic structure and real projective structure. In *SPM '06: Proceedings of the 2006 ACM Symposium on Solid and Physical Modeling*, 105–116.

JIN, M., KIM, J., LUO, F., AND GU, X. 2008. Discrete surface ricci flow. *IEEE TVCG 14*, 5, 1030–1043.

JIN, M., ZENG, W., LUO, F., AND GU, X. 2008. Computing teichmüller shape space. *IEEE TVCG 99*, 2, 1030–1043.

KRAEVOY, V., AND SHEFFER, A. 2004. Cross-parameterization and compatible remeshing of 3d models. *ACM Transactions on Graphics 23*, 3, 861–869.

LÉVY, B., PETITJEAN, S., RAY, N., AND MAILLOT, J. 2002. Least squares conformal maps for automatic texture atlas generation. *SIGGRAPH 2002*, 362–371.

LI, X., BAO, Y., GUO, X., JIN, M., GU, X., AND QIN, H. 2008. Globally optimal surface mapping for surfaces with arbitrary topology. *IEEE TVCG 14*, 4, 805–819.

LUO, F. 2004. Combinatorial yamabe flow on surfaces. *Commun. Contemp. Math. 6*, 5, 765–780.

MERCAT, C. 2004. Discrete riemann surfaces and the ising model. *Communications in Mathematical Physics 218*, 1, 177–216.

PINKALL, U., AND POLTHIER, K. 1993. Computing discrete minimal surfaces and their conjugates. *Experimental Mathematics 2*, 1, 15–36.

TEWARI, G., GOTSMAN, C., AND GORTLER, S. J. 2006. Meshing genus-1 point clouds using discrete one-forms. *Comput. Graph. 30*, 6, 917–926.

TONG, Y., ALLIEZ, P., COHEN-STEINER, D., AND DESBRUN, M. 2006. Designing quadrangulations with discrete harmonic forms. In *SGP '06: Proceedings of the fourth Eurographics symposium on Geometry processing*, 201–210.

TONG, Y., ALLIEZ, P., COHEN-STEINER, D., AND DESBRUN, M. 2006. Designing quadrangulations with discrete harmonic forms. In *Symposium on Geometry Processing*, 201–210.

WANG, Y., GUPTA, M., ZHANG, S., WANG, S., GU, X., SAMARAS, D., AND HUANG, P. 2005. High resolution tracking of non-rigid 3d motion of densely sampled data using harmonic maps. In *ICCV*, 388–395.

WANG, S., WANG, Y., JIN, M., GU, X. D., AND SAMARAS, D. 2007. Conformal geometry and its applications on 3d shape matching, recognition, and stitching. *IEEE Trans. Pattern Anal. Mach. Intell. 29*, 7, 1209–1220.

WEITRAUB, S. H. 2007. *Differential Forms: A Complement to Vector Calculus*. Academic Press.

XU, G. 2008. Finite element methods for geometric modeling and processing using general fourth order geometric flows. In *GMP*, 164–177.

YIN, X., DAI, J., YAU, S.-T., AND GU, X. 2008. Slit map: Conformal parameterization for multiply connected surfaces. In *Advances in Geometric Modeling and Processing, 5th International Conference, GMP*, Springer, vol. 4975 of *Lecture Notes in Computer Science*, 410–422.

ZENG, W., YIN, X., ZENG, Y., WANG, Y., GU, X., , AND SAMARAS, D. 2008. 3d face matching and registration based on hyperbolic ricci flow. In *CVPR 2008 Workshop on 3D Face Processing*.

ZENG, W., ZENG, Y., WANG, Y., YIN, X., GU, X., AND SAMARAS, D. 2008. 3d non-rigid surface matching and registration based on holomorphic differentials. In *The 10th European Conference on Computer Vision (ECCV) 2008*, 1–14.

ZENG, W., JIN, M., LUO, F., AND GU, X. 2009. Canonical homotopy class representative using hyperbolic structure. In *IEEE SMI*.

ZENG, W., LUI, L.-M., GU, X., AND YAU, S.-T. 2009. Shape analysis by conformal modules. *Methods and Applications of Analysis*.

A Theories of Generalized Koebe's Method

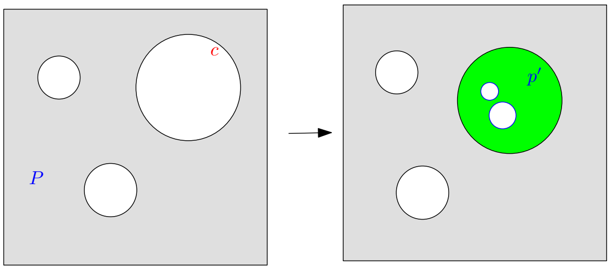

Figure 14: A circle domain P and Schwarz reflection.

A.1 Conformal Mapping for Circle Domain

A circle domain P is a domain in $\hat{C}$ bounded by round circles, as shown in Figure 14. We assume that $\infty \in P$ and $|z| = 1$ is a boundary of P. Give a circle domain P and a component C of ∂P, we can use Schwartz reflection to reflect P about C to produce a new circle domain P'. We call P' a level-1 copy of P. There are n level-1 copies of P if P has n boundary components.

We can reflect P' about its boundary circles to get level-2 copies of P. In doing so, we obtain a Schottky picture of P shown in Figure 15. It is well known that the boundary circles of level-k are disjoint and bound an area $< C_1$, C_1 depends only on P.

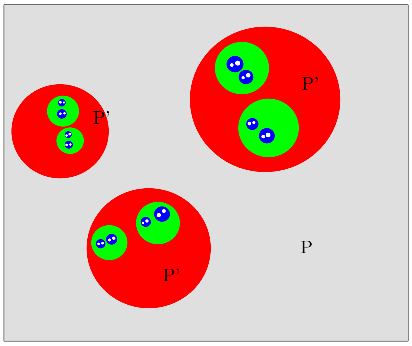

Figure 15: Schottky picture of P. Red regions are level-1 copies of P, green regions level-2 copies of P, blue regions are level-3 copies of P.

Let P_k be the union of P together with all level $\leq k$ copies of P.

Theorem A.1 (Henrici). *There exist two constants $C_1, C_2 > 0, C_1 < 1$, so that if $\phi : P \to \hat{C}$ is an analytic embedding with $\phi(z) = z + O(\frac{1}{z}), z \to \infty$, sending $|z| = 1$ to $|z| = 1$ and ϕ can be extended to be an analytic embedding to P_k, then $|\phi(z) - z| \leq C_2 C_1^k$ for all $z \in P$*

The proof is to use Cauchy integral formula in the domain P_k and use area estimate. (see page 502-505 in [Henrici 1993])

A.2 Koebe's Iteration and Convergence

Given a multiply connected domain R, say $\infty \in int(R)$, there exists a circle domain P and analytic homeomorphism $f : P \to R$, as shown in .

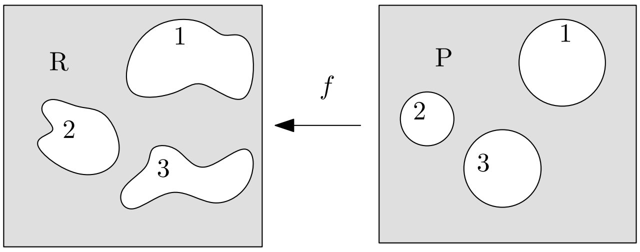

Figure 16: Conformal mapping from the circle domain to the multiply connected domain.

To approximate f Koebe tries to "renormalize" R by make a boundary component a round circle, one at a time. We may assume $\partial R = C_1 \cup C_2 \cup C_3$ and C_i analytic Jordan curves: Let D_i be the disk bounded by c_i Let be $h_1 : D_1^c \to \{|z| > 1\} \cup \{\infty\}$ be the normalized Riemann mapping ($h_1(z) = z + o(\frac{1}{z})$).

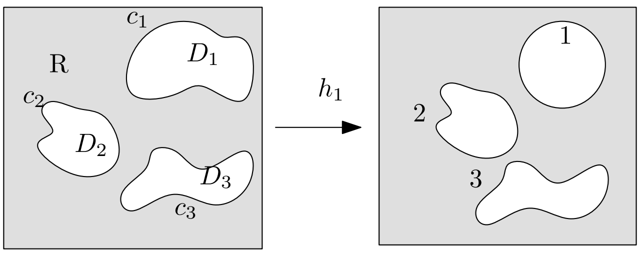

Key observation of Koebe: the composition: $h_1 \circ f : P \to h_1(P)$ sends one boundary component of P to the circle $h_1(C_1)$. Thus by Schwartz reflection principle, $h_1 \circ f$ extends to $P \cup P' \to \hat{C}$ where P' is a level-1 copies of P. See the green region in the following figure.

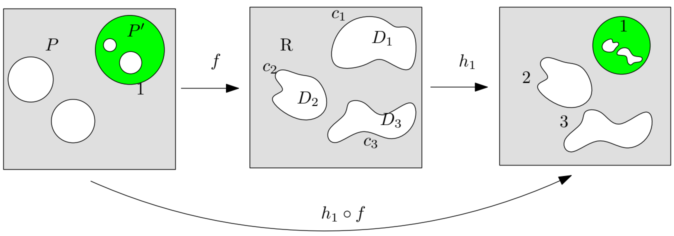

Now, let us use Riemann mapping h_2 for the 2nd computation of $h_1(R)$. Now, $h_2 \circ h_1 \circ f$ is defined on $P \cup P'$, i.e. $h_2|_{h_1 \circ f(P')}$ is defined. See the green region in the following figure.

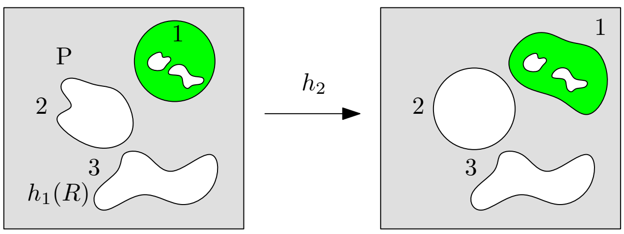

Also $h_2 \circ h_1 \circ f$ sends the second circle boundary of P to a circle. Thus $h_2 \circ h_1 \circ f$ using Schwartz reflection, can be extended to $P \cup P' \cup P''$ where P'' is another level-1 copy, shown as yellow region in the following figure.

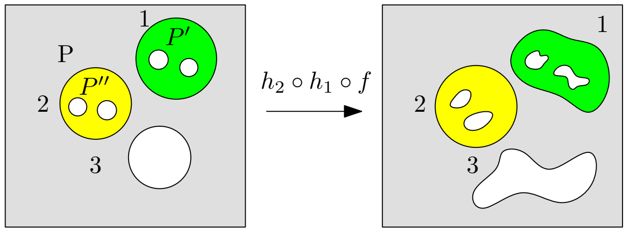

The more Riemann mapping h_k we use to normalize the boundary components of $h_{k-1}h_{k-2}....h_1(R)$, the higher level-copies that we can extend $h_k \circ ..... \circ h_1 \circ f$ from $P \to \hat{C}$ to $P_{\frac{k}{3}} \to \hat{C}$. By theorem A.1,

$$|h_k \circ ...... \circ h_1 \circ f(z) - z| < C_2 C1^{[\frac{k}{3}]}, \tag{4}$$

namely it produces a better and better approximation to f^{-1}.

A.3 Generalized Koebe's Method

Now it is clear that if one normalizes pair of boundary components C_1, C_2 of R, one at a time, the process will converge faster.

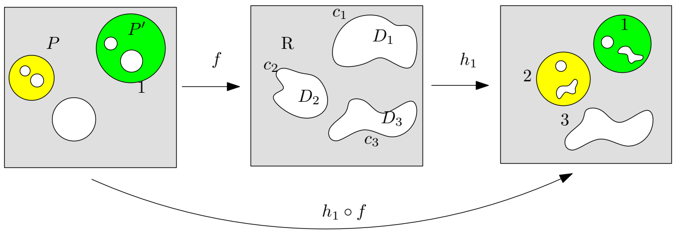

Given a multiply connected domain R, P is the circle domain, $f : P \to R$ is a conformal mapping. Just like Koebe's case, one sees that

$$h_k \circ h_{k-1} \circ ...... \circ h_1 \circ f : P \to \hat{C}$$

can be extended to $P \cup Q_1 \cup ... \cup Q_k$, where Q_i are obtained by Schwartz reflection of copies of P. After k steps, the mapping $h_k \circ \cdots \circ h_1 \circ f$ from $P \to \hat{C}$ can be extended to $P_{\frac{2k}{3}} \to \hat{C}$, by theorem A.1,

$$|h_k \circ h_{k-1} \circ ...... \circ h_1 \circ f(z) - z| < C_1 C_2^{2[\frac{k}{3}]}. \tag{5}$$

Compareing the Equation 4 and 5, it is clear that generalized Koebe's method converges quadratically faster than the conventional Koebe's method.

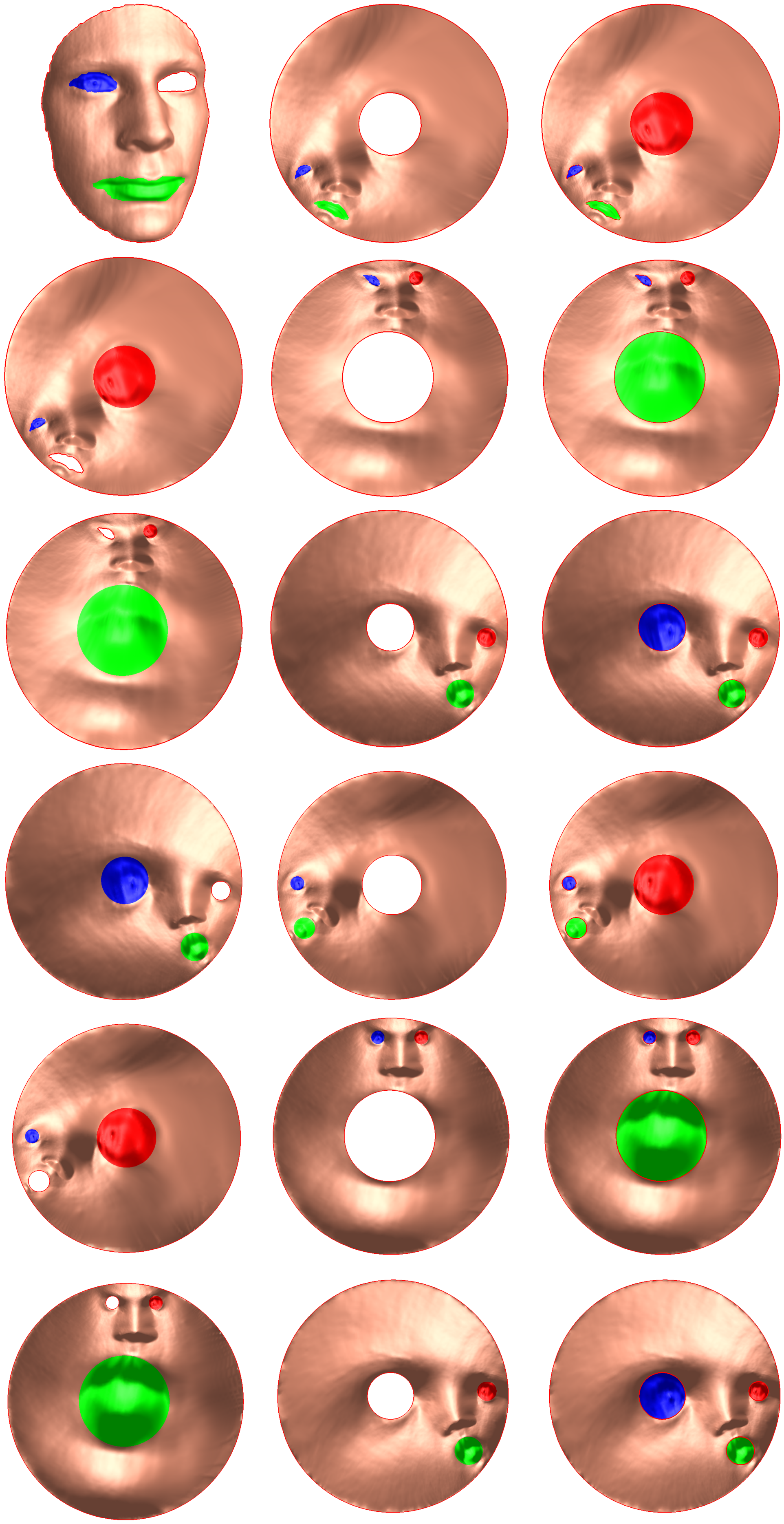

Step (1)

Step (2)

Step (3)

Step (4)

Step (5)

Step (6)

(a) Choose two boundaries (b) Riemann mapping (c) Fill holes

Figure 9: Koebe's method for computing conformal maps for multiply connected domains.